Int. J. Heat Mass Transfer. Vol. 34, No. 7, pp. 1811–1822, 1991
Printed in Great Britain

0017–9310/91 $3.00+0.00

Three-dimensional heat transfer and fluid flow in the modern discharge lamp

P. Y. CHANG† and W. SHYY‡

† Advanced Technology Department, G.E. Lighting, Cleveland, OH 44112, U.S.A.
‡ Department of Aerospace Engineering, Mechanics and Engineering Science, University of Florida, Gainesville, FL 32611, U.S.A.

(*Received* 1 *May* 1990 *and in final form* 11 *September* 1990)

Abstract—It is well established that heat transfer and convection characteristics can substantially affect the light quality as well as life expectancy of a discharge lamp. However, the present level of understanding of these processes is not adequate to guide engineering design due to the combined physical and geometrical complexities involved. Efforts have been made both experimentally and theoretically in the present work to identify the roles of different heat transfer mechanisms between the arctube and the jacket of a modern discharge lamp. By solving the three-dimensional Navier–Stokes equations and a simplified radiation model in curvilinear coordinates, good agreement between measurements and predictions in terms of the wall temperature profiles have been obtained. Both convection and radiation modes are found important in overall heat transfer. Interplays between temperature gradients and geometrical variations around the arctube, and their impact on the structure of the convection field inside the jacket have also been revealed in a detailed manner by the theoretical model.

1. INTRODUCTION

THE DISCHARGE lamp is an important light source for general illumination [1, 2]. It usually utilizes two electrodes, contained in a small quartz tube which is, in turn, embedded in a much larger glass jacket. The quartz tube is filled with mercury and often with metal halide additives as the major and minor species. Within the tube, the electric discharge vaporizes these species to form an arc of high temperature, up to 7000 K, and high pressure, of several atmospheres. Figure 1 illustrates a modern design which depicts a curved arctube contained in an outer jacket filled with nitrogen. Due to its technical and commercial importance, and the intrinsic physical and chemical complexities, considerable research has been conducted into various areas relevant to the design of the discharge lamp. Among many important issues, natural convection has received increasing emphasis since a critical requirement for designing a high quality discharge lamp is to distribute its wall temperature as evenly as possible in order to maximize metal halide vapor pressure, which is largely determined by the temperature of the coldest region of the arctube. The degree of uniformity of temperature distribution, both within the arctube and on its solid wall, can greatly affect the light quality as well as life expectancy of the lamp.

Kenty [3] conducted the first experimental research into natural convection inside a discharge arctube. Zollweg [4] and Lowke [5] were the first to conduct the analytical and computational studies of natural convection in high pressure mercury arcs. In their works, the fluid flow and energy equations in an axisymmetric domain were solved. Dakin and Shyy [6] developed a more comprehensive and detailed model to study the vertical metal halide discharge by including two-dimensional transport of the convection, the electric field, demixing of different species, and radiation.

More recently, progress has been made in three-dimensional computation modeling of thermofluid flow processes in the discharge [7–10] with a capability of handling the complex geometry of the arctube,

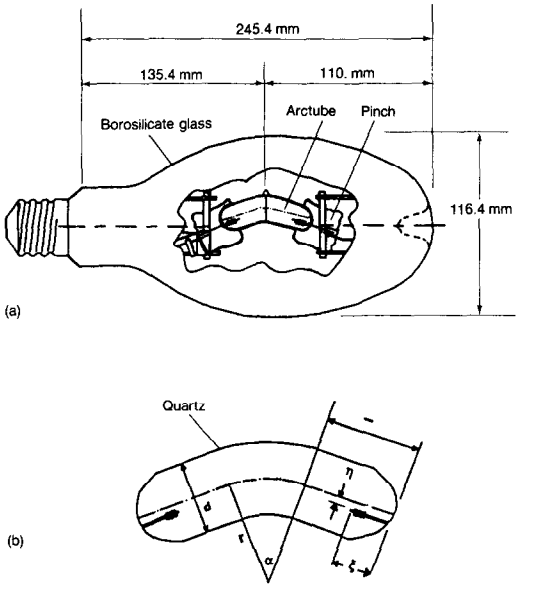

FIG. 1. (a) Jacket geometry. (b) Arctube geometry.

including the curved surface and electrode insertion. The model advanced in refs. [7–10] solves the combined momentum, mass continuity, energy, and electric field equations, based on the fundamental conservation laws, and a simplified radiation heat transfer model. A finite volume algorithm based on general non-orthogonal curvilinear coordinates has been adopted in numerical computation. Good agreement between experimental measurements and theoretical prediction has been obtained in terms of mounting angle, curvature effect, and the wall temperature distribution. Results presented in refs. [7–10] appear to be the first successful theoretical modeling of the very complicated three-dimensional transport phenomena in a discharge arctube. Much new insight has been gained from these studies. It is noted that the model used in refs. [7–10] considered that the arctube was contained in a vacuum jacket, and the convection process between jacket and arctube was excluded.

In the present work, advancement has been made toward modeling and predicting the heat transfer and associated fluid flow characteristics between the arctube and the jacket. For this problem, the electric field does not appear since there is no current flow through the outer jacket gas. However, the geometry is complicated and contains curved surfaces for both the outer boundary, i.e. the jacket, and inner obstacle, i.e. the arctube. It poses a challenge to the computational techniques to faithfully incorporate these geometric characteristics into a fundamental model based on first principles.

For the present work both experimental and theoretical information has been collected to study the heat transfer and associated fluid flow characteristics. Experimentally, wall temperature distributions of both arctube and jacket have been obtained, either with a nitrogen filled jacket or with a vacuum jacket. On the theoretical side, a three-dimensional model has been developed including treatment of the Navier–Stokes equations to account for the convection and conduction effects between the arctube and the jacket surfaces, the conduction equation to account for the heat transfer across the jacket wall, and a simplified radiation model to account for wall to wall radiation heat transfer between the arctube and the jacket. The relative contributions between convection and radiation to the overall arctube-to-jacket heat transfer have been identified. Good agreement between theory and data has been obtained, and therefore a detailed assessment of the physical mechanisms responsible for the observations can be given.

2. LAMP GEOMETRY AND PROBLEM FORMULATION

The geometrical definition of a particular modern discharge lamp, including both the arctube and jacket, is given in Fig. 1 and Table 1. In this design, the arctube is bowed to accommodate the upward biased temperature profiles caused by natural convection [7].

Table 1. Arctube geometry

Symbol	Geometric design parameters	400 W data
d	arctube diameter (mm)	15.1
l	arctube length (mm)	59.3
ξ	electrode insertion length (mm)	9.3
η	offset electrode distance (mm)	2.3
r	radius of bend (mm)	25.4
α	angle of bend (deg)	40.0
t	wall thickness (mm)	1.2

Accordingly, the mounting orientation of a lamp has a definite impact on its performance and life expectancy [8]. The lamp shown in Fig. 1 is specially designed for horizontal mounting and is often used in turnpike, street or billboard lighting. The outer jacket approximates an ellipsoid, with a cylindrical neck region. Between the arctube and the jacket, there are wiring and supporting structures to position the arctube as well as to supply electric power. Since these auxiliary structures are of negligible physical dimensions in comparison to the arctube and outer jacket, their presence is not accounted for in the present model. A three-dimensional illustration of the grid system generated and utilized in our computations is shown in Fig. 2, where $31 \times 19 \times 19$ and $17 \times 5 \times 5$ grid points are employed to represent the jacket and the arctube, respectively.

Conduction, convection, and radiation effects are included in regions where these effects are important. For the general fluid flow field, the Navier–Stokes equations are adopted. The governing equations are first written in the strong conservation law form in Cartesian coordinates for the general dependent variable ϕ

$$\frac{\partial}{\partial x}(\rho u\phi)+\frac{\partial}{\partial y}(\rho v\phi)+\frac{\partial}{\partial z}(\rho w\phi)=\frac{\partial}{\partial x}\left(\Gamma\frac{\partial\phi}{\partial x}\right)+\frac{\partial}{\partial y}\left(\Gamma\frac{\partial\phi}{\partial y}\right)+\frac{\partial}{\partial z}\left(\Gamma\frac{\partial\phi}{\partial z}\right)+R(x,y,z). \quad (1)$$

Here, Γ is the effective diffusion coefficient and R the source term, including the gravitational force and pressure gradients in the momentum equation. Equation (1) can represent the continuity, momentum, and

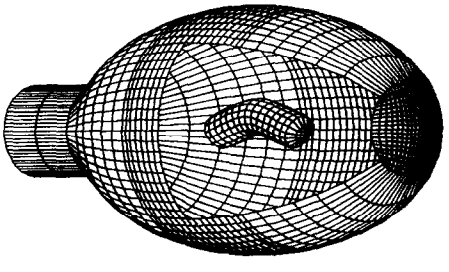

Mesh of jacket – $31 \times 19 \times 19$

Mesh of arctube – $17 \times 5 \times 5$

FIG. 2. Computer generated geometry and mesh (in three-dimensional perspective).

energy equations. When new independent variables ξ, η, and γ are introduced, equation (1) changes according to the general transformation $\xi = \xi(x, y, z)$, $\eta = \eta(x, y, z)$, $\gamma = \gamma(x, y, z)$. The result of this coordinate transformation is to transform the arbitrarily shaped physical domain into a rectangular parallelepiped.

To resolve the geometrical complexities of the arctube and jacket, the coupled set of transport equations are solved by an algorithm using general nonorthogonal curvilinear coordinates [11–13], and a finite volume formulation has been employed for all first-order derivatives including convection and pressure terms. In the present formulation, the gas temperature between the arctube and the jacket is around several hundred Kelvin, and the gaseous radiative heat transfer is negligible. The radiation heat transfer between the arctube wall, made of quartz, and the jacket wall, made of borosilicate glass, however, is important and must be accounted for. Even though computational methods are available to account for the radiation heat transfer in more detailed manners [14, 18], in view of the geometrical complexities studied here, it would be computationally prohibitive to adopt them. Instead, a much simplified model has been adopted. The arctube is considered to be a point source radiating energy toward the jacket wall. Each mesh area on the solid surface of the jacket is assumed to receive the radiant energy from the arctube; the amount of energy absorption among those meshes is determined according to the following procedure:

(i) The energy emitted from the arctube wall, Q_e, is first computed as follows:

$$Q_e = \sigma\varepsilon[(T_{wo})^4_{arctube} - (T_{wi})^4_{jacket}]A_{arctube} \tag{2}$$

where σ is the Stefan–Boltzmann constant, ε the quartz emissivity, $(T_{wo})_{arctube}$ the outer wall temperature of the arctube, $(T_{wi})_{jacket}$ the inner wall temperature of the jacket, and $A_{arctube}$ the arctube outer wall surface area.

(ii) The radiative heat flux, q_i, into each computational mesh of the inner wall of the jacket is then determined by the following formulas:

$$Q_a = CQ_e \tag{3}$$

$$w_i = A_i/r_i^{\alpha} \tag{4}$$

$$q_i = Q_a \frac{w_i}{\Sigma w_i} \Big/ A_i \tag{5}$$

where Q_a is the net energy absorbed by the jacket wall through radiation, C the fraction of arctube radiated energy absorbed by the jacket wall, which is taken here as 0.9, Σ the summation over all the meshes on the inner wall of the jacket, w_i the weighting factor of each mesh, A_i the mesh area i on the inner wall of the jacket, α a constant to be determined, and r_i the distance between the point source representing the arctube and the center of mesh i. The exact location of the point source is also to be determined. It should be noted that the arctube is not geometrically centered.

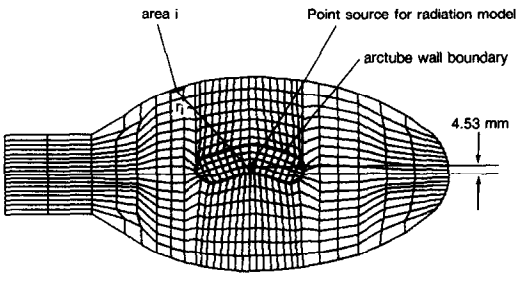

FIG. 3. Radiation model.

A schematic illustration of the present simplified radiation model is given in Fig. 3. If the outer jacket is of a spherical shape, then $\alpha = 2$. Otherwise, an effective value of α and the location of the point source need to be determined to account for the geometrical irregularity. This issue will be addressed later. Heat transfer across the jacket wall has also been accounted for in our model. The temperature distribution on both the inner and outer walls of the jacket can be determined by balancing the energy transfer as follows:

(i) Inner wall temperature of the jacket, $(T_{wi})_{jacket}$ is computed by balancing (a) energy transmitted to the wall by nitrogen contained inside the jacket, (b) radiant energy absorbed by the inner wall of the jacket, and (c) heat conduction across the jacket wall, i.e.

$$-k_{gas}\frac{(T_{wi})_{jacket} - T_P}{\delta} + q_i = -k_{jacket}\frac{(T_{wo})_{jacket} - (T_{wi})_{jacket}}{t} \tag{6}$$

where k_{gas} and k_{jacket} are, respectively, the thermal conductivities of the nitrogen gas contained in the jacket and the borosilicate glass of the jacket, both are functions of temperature, $(T_{wi})_{jacket}$ and $(T_{wo})_{jacket}$ are, respectively, the inner and outer wall temperatures of the jacket, T_P the temperature at the center of the fluid control volume in the gas phase next to the inner wall of the jacket, δ the normal distance from the center of the fluid control volume to the inner wall of the jacket, and q_i the radiative heat flux defined by equation (5).

(ii) Outer wall temperature of the jacket, $(T_{wo})_{jacket}$, is computed by balancing (a) heat conduction to the outer jacket wall from the inner wall, and (b) energy radiated and convected to the atmosphere, i.e.

$$-k_{jacket}\frac{(T_{wo})_{jacket} - (T_{wi})_{jacket}}{t} = \sigma\varepsilon[(T_{wo})^4_{jacket} - T^4_{sink}] + h[(T_{wo})_{jacket} - T_{sink}] \tag{7}$$

where T_{sink} is the room temperature and h the heat transfer coefficient. Physical properties of the nitrogen gas and borosilicate glass are taken from refs. [16, 17],

respectively. Based on an order of magnitude analysis, it is sufficient for the present application to consider only one-dimensional heat conduction across the jacket wall.

With regard to other necessary boundary conditions, the standard no-slip condition is enforced for velocity variables along both the outer wall of the arctube and the inner wall of the jacket. The outer wall temperature of the arctube is prescribed according to experimental information. Due to the nature of the staggered grid arrangement adopted in the computational algorithm, there is no need to supply any artificial boundary conditions to the continuity (i.e. pressure-correction) equation. Extrapolation is adopted for the necessary pressure gradient terms in the boundary treatment portion of the momentum equations. For all the derivatives in the transport equations, convection included, the second-order central differencing schemes are employed for discretization. A multigrid method is utilized for solving the resulting difference equations. Various aspects of the numerical techniques can be found in refs. [11–13].

3. RESULT AND DISCUSSION

We first present some experimental information on the measured wall temperatures of lamps specially made to aid our present effort. Two types of 400 W lamps were manufactured, one with a standard jacket, i.e. a nitrogen filled one, and the other with an evacuated jacket. For the nitrogen filled lamp, the pressure inside the jacket at room temperature, i.e. without turning on the power, was 380 Torr. In both types, the arctube was curved and filled with mercury only, as in refs. [7–10]. Temperature measurements of both the outer jacket wall and the outer arctube wall were made. Hence the relative impact of radiative and convective heat transfer between arctube and jacket can be unequivocally separated.

The outer wall temperature of the jacket was measured using a thermocouple. Figure 5(a) shows where the measurements were made. The outer wall temperature of the arctube was measured using an Ircon radiation pyrometer, an optical device which can quantitatively measure the radiance of a blackbody or other radiant object. Aquadag is applied on the locations where the temperature measurements are desired. Each aquadag spot is about 2 mm in size and is opaque. To take measurements, a frontal surface mirror is used to sight the aquadag spots. Then the radiant measurements obtained from the radiation pyrometer are converted to temperature by calibration.

The particular lamp studied in the current work is of 400 W power input. Figure 4 shows the measured outer wall temperature profiles of the arctube within the vacuum and nitrogen filled jackets. The maximum temperture is around 920°C. It is reported in ref. [8] that inside the arctube, the peak gas temperature is around 6700 K and the pressure is around 3 atm. Figure 5(b) shows the direct comparison of the top and bottom outer wall temperatures of the jacket for both nitrogen filled and vacuum conditions inside the jacket. The position of peak temperature corresponds to the center of the arctube, which indicates the effect of arctube curvature on the jacket wall temperature distribution. It is noted that the jacket itself is axisymmetric but the arctube is not.

For the vacuum jacket (dotted lines), the differences between top and bottom wall temperatures are caused by location and geometry of the arctube. The variations in geometry and view angle also cause the nonuniform temperature distribution in the axial direction on both top and bottom jacket walls. For the nitrogen filled jacket, natural convection makes a substantial impact on the jacket wall temperature distribution. The average wall temperature of the arctube is much higher than the jacket wall temperature. Consequently, natural convection induced by the temperature nonuniformity heats up the top wall and cools down the bottom wall of the jacket. Details of the natural convection process cannot be deduced simply from the wall temperature measurements and will be investigated later based on the theoretical computation.

The theoretical model presented in the previous section does not need any artificially adjusted parameters except for the exponent α in equation (4) and the location of the point source. A series of numerical computations has been conducted for the vacuum jacket which includes radiation between arctube and jacket walls, and conduction across the jacket wall, but excludes convection. The values of ε and A_{arctube} in equation (2) are 0.5 and 35.5 cm^2, respectively. Based on equation (2) and the measured data, the energy emitted from the arctube wall, Q_e, is 155 W for the vacuum jacket case and 138 W for the nitrogen filled jacket case.

The value of α in equation (4) and the point source position could then be decided by finding the best match between predicted and measured outer jacket wall temperature distributions. As demonstrated in Fig. 6(a), it is found that the combination of $\alpha = 2.8$ and the point source location being 4.53 mm above the jacket axis (as shown in Fig. 3) gives very good agreement between theoretical model prediction and experimental measurement for both top and bottom wall temperature profiles; in fact, they agree within the experimental uncertainties. Figure 6(b) illustrates the sensitivity of predicted jacket wall temperatures with respect to the variation of α in equation (4), from $\alpha = 2.0$ to 3.5. Substantial differences are observed between the two predictions. Nevertheless, it is clearly demonstrated here that even though the present point source model is extremely simple, it does a surprisingly good job to represent the distribution and the effect of radiation heat transfer. It is concluded that this approach is a good compromise between representing the physics and optimizing the computational require-

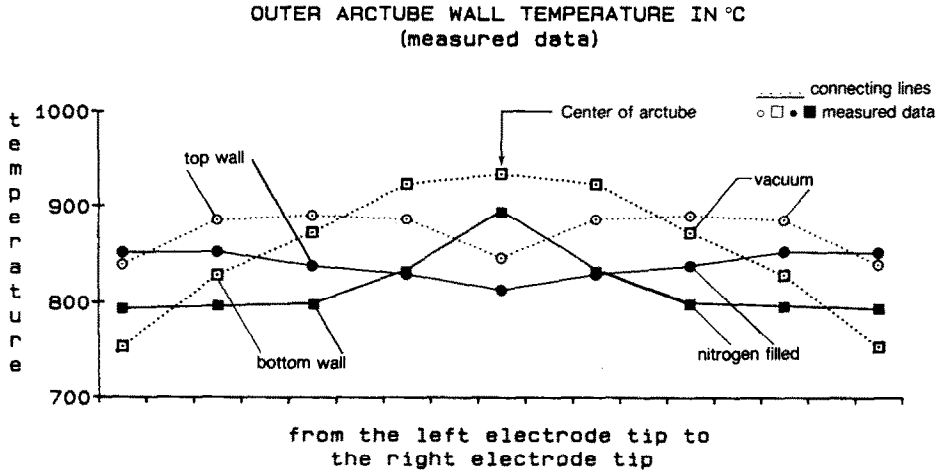

FIG. 4. Measured outer wall temperature of arctube with vacuumed and nitrogen filled jacket conditions.

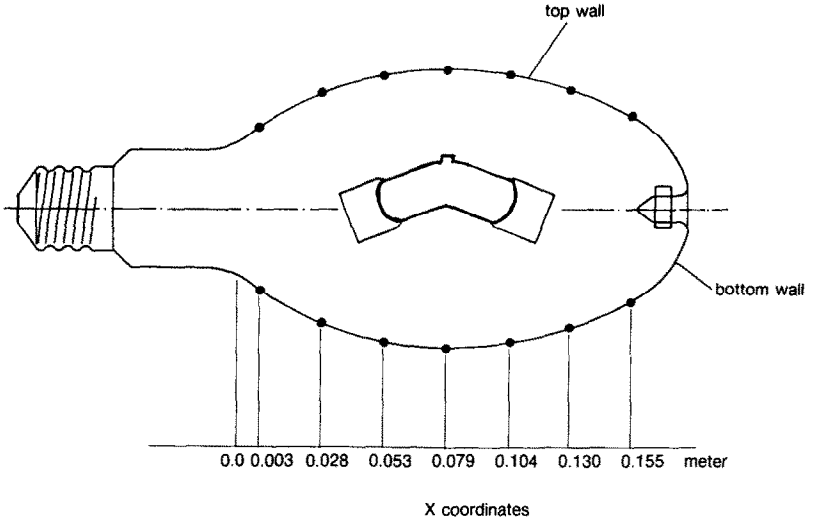

FIG. 5(a). x coordinates of locations '●' where measurements are taken.

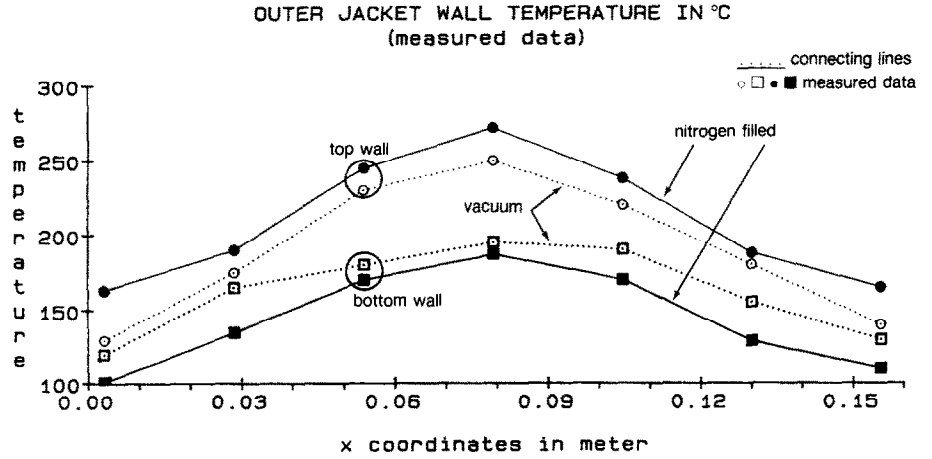

FIG. 5(b). Measured outer wall temperatures of jacket between vacuum and nitrogen filled conditions.

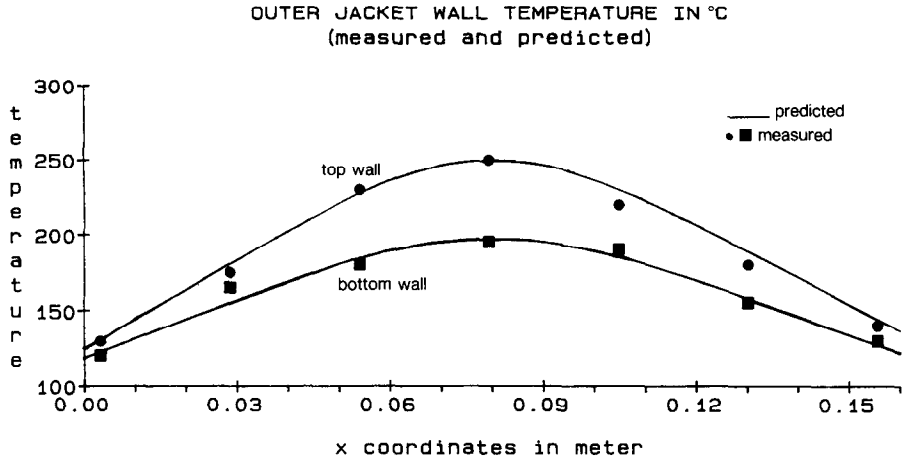

FIG. 6(a). Comparison of predicted and measured outer wall temperature of vacuumed jacket with optimized α in equation (4).

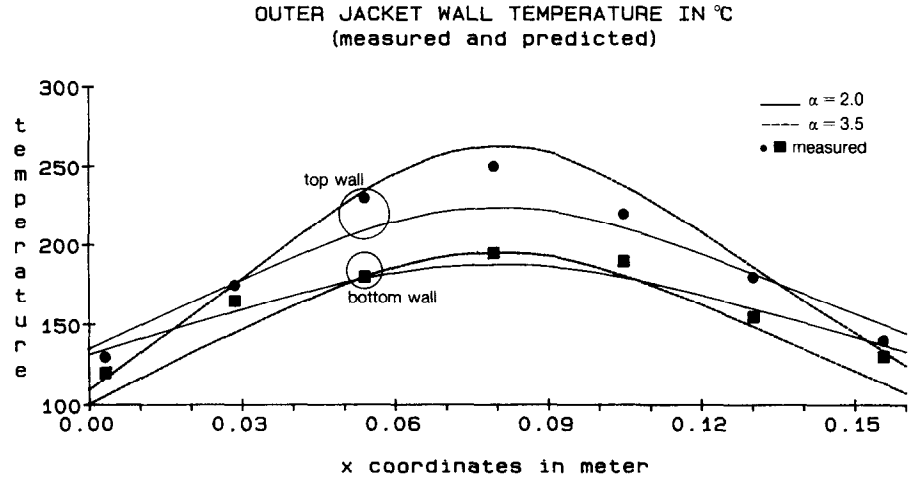

FIG. 6(b). Sensitivity of wall temperature prediction of vacuumed jacket to α in equation (4).

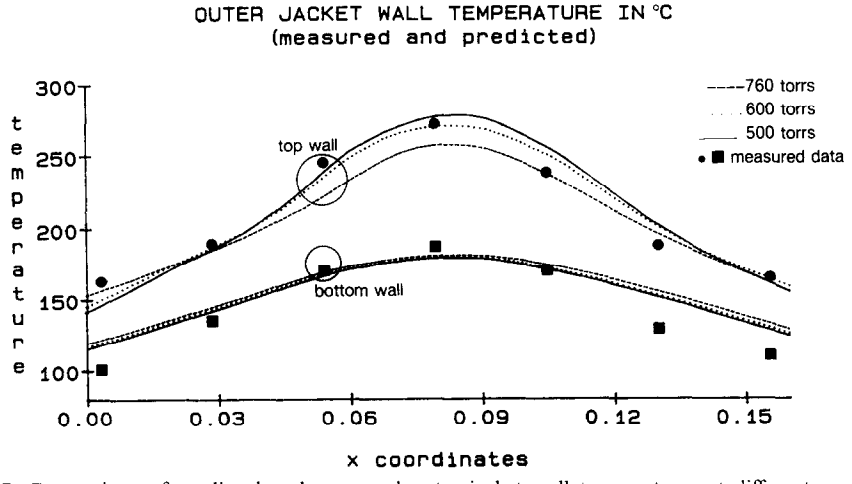

FIG. 7. Comparison of predicted and measured outer jacket wall temperatures at different operating pressures.

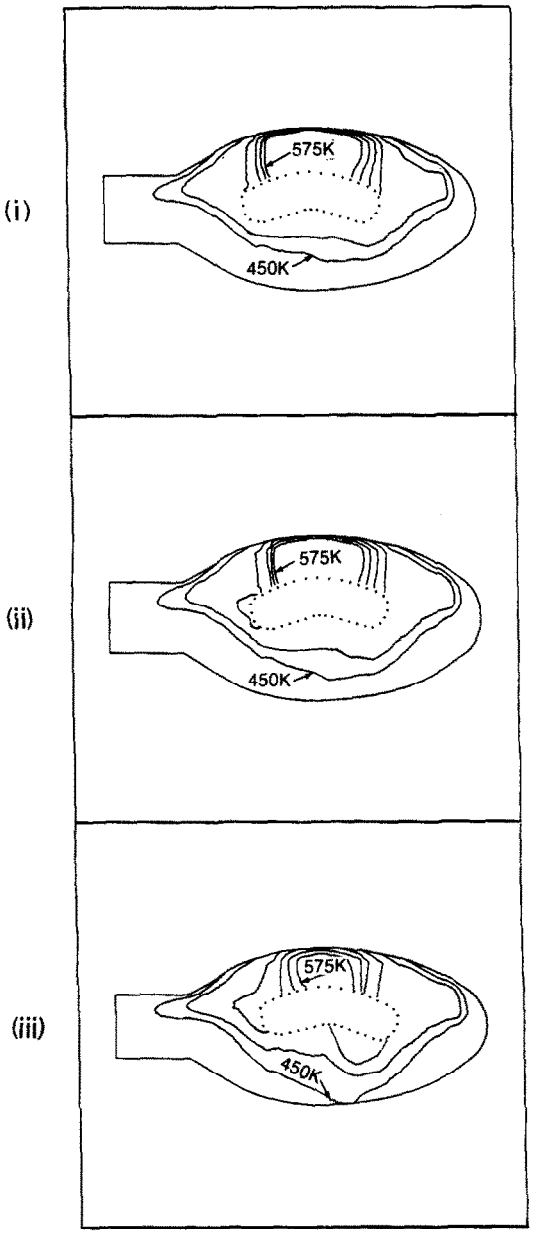

FIG. 8(a). Temperature contours in middle side-view plane corresponding to three operating pressures inside the jacket: (i) 500 Torr; (ii) 600 Torr; (iii) 760 Torr (contour intervals = 25 K).

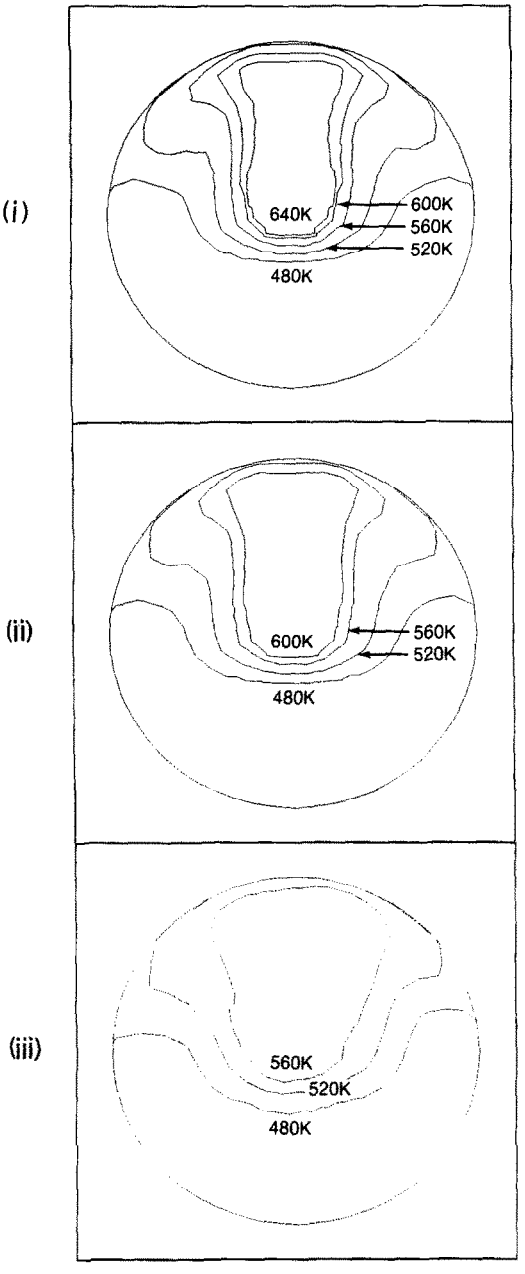

FIG. 8(b). Temperature contours in middle cross-view plane corresponding to three operating pressures inside the jacket: (i) 500 Torr; (ii) 600 Torr; (iii) 760 Torr.

ments. In all the following discussions, the value of α is fixed at 2.8 and also the point source location is fixed as shown in Fig. 3.

By adequately representing the radiation part of heat transfer, the effect of convection can then be predicted and appraised against the experimental information. Detailed assessments can also be made of the interplay between different heat transfer modes as well as its impact on natural convection. For the cases presented below, gravity is perpendicular to the axisymmetric axis of the jacket configuration, i.e. the lamp is positioned horizontally. The outer wall temperature profiles of the arctube adopted in the calculations were based on the measurements shown in Fig. 4. Nitrogen is filled into the jacket at 380 Torr under cold conditions, i.e. room temperature. Here a parametric variation of *operating* (not cold fill) pressure has been conducted in the theoretical model to study its effect on overall heat transfer. Steady-state solutions could be obtained for operating pressures up to 680 Torr, above which the model predicts that oscillatory solution characteristics start to appear.

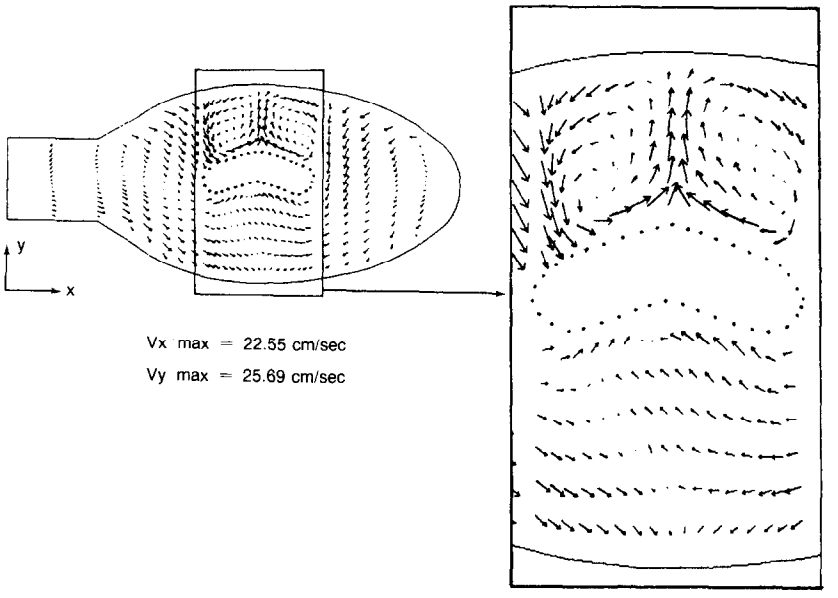

FIG. 9. Velocity vectors in middle side-view plane for operating pressure of 600 Torr.

The unsteadiness increases with increasing operating pressure. In terms of jacket wall temperature, the unsteadiness of the flow field does not show noticeable impact up to the highest pressure, 1000 Torr, considered here. The detailed nature of the oscillations is not our focal point here. Suffice it to note that the growing unsteadiness in solution with increasing pressure is expected simply from the viewpoint that the Rayleigh number increases with pressure.

Figure 7 compares the predicted and measured top and bottom outer jacket wall temperatures where the predictions were made based on three operating pressures inside the jacket, namely, 500, 600, and 760 Torr. It is clear that as the pressure increases the strength of natural convection increases. With increasing pressure, convection causes the gas temperature to be more uniformly distributed inside the jacket as shown by Figs. 8(a) and (b). Consequently, in the region directly above the arctube the wall temperature decreases as pressure increases, while the region close to the end zone, the wall temperature increases with increasing pressure. For the bottom wall temperature, on the other hand, increasing jacket pressure causes it to increase monotonically, but only to a modest extent. Figure 8(b) also shows that in the cross-view planes, the temperature distribution is symmetric at 500 and 600 Torr, but becomes asymmetric at 760 Torr. It is noted that at 760 Torr, no convergent steady state solution could be obtained; the isotherms shown in Fig. 8 are representative but they are not from a convergent solution.

Figures 9 and 10 depict selected plots of the velocity field on several side- and cross-view planes to illustrate more detailed information regarding the convection field induced by the temperature nonuniformities. A pair of contrarotating convection cells above the arctube can be clearly identified in the middle side-view plane. Figure 9 shows that, in the side-view plane of symmetry and above the middle of the arctube, high temperature combined with upward curving of the tube wall creates a thermal plume type of flow which moves to the top surface of the jacket, then turns to opposite directions to form two large scale recirculating eddies. The downward entrainment in regions close to the two ends of the arctube induced by the afore-mentioned contrarotating cells are large enough to have the fluid penetrate into the domain around and beneath the arctube, where multiple recirculating eddies are also present.

Figure 10 shows a series of velocity vector plots in cross-view planes, from Plane No. 5 to Plane No. 27. It is noted that Plane No. 17 is the one cutting through the cross-view plane of symmetry of the *arctube*. The flow structures are obviously three-dimensional and complicated. The top wall temperature of the arctube which is around 800°C, is consistently much higher than the top wall temperature of the jacket, which is around 200°C. Furthermore, according to Figs. 4 and 5, their difference is higher than those along the top wall of the arctube. However, as far as convection is concerned, the flow development in the side-view planes seems to dominate that in the cross-view planes.

For example, despite the fact that all the gas particles above the arctube are heated from below, they do not always move upward. Figure 10 shows that the gas particles above the arctube but close to the end regions of the arctube, as in cross-view Planes No. 9, 11, and 25, actually move downward. On the other hand, the gas particles above the middle of the arctube, as in cross-view Planes No. 15, 17, and 19, move upward. This phenomenon is apparently caused by

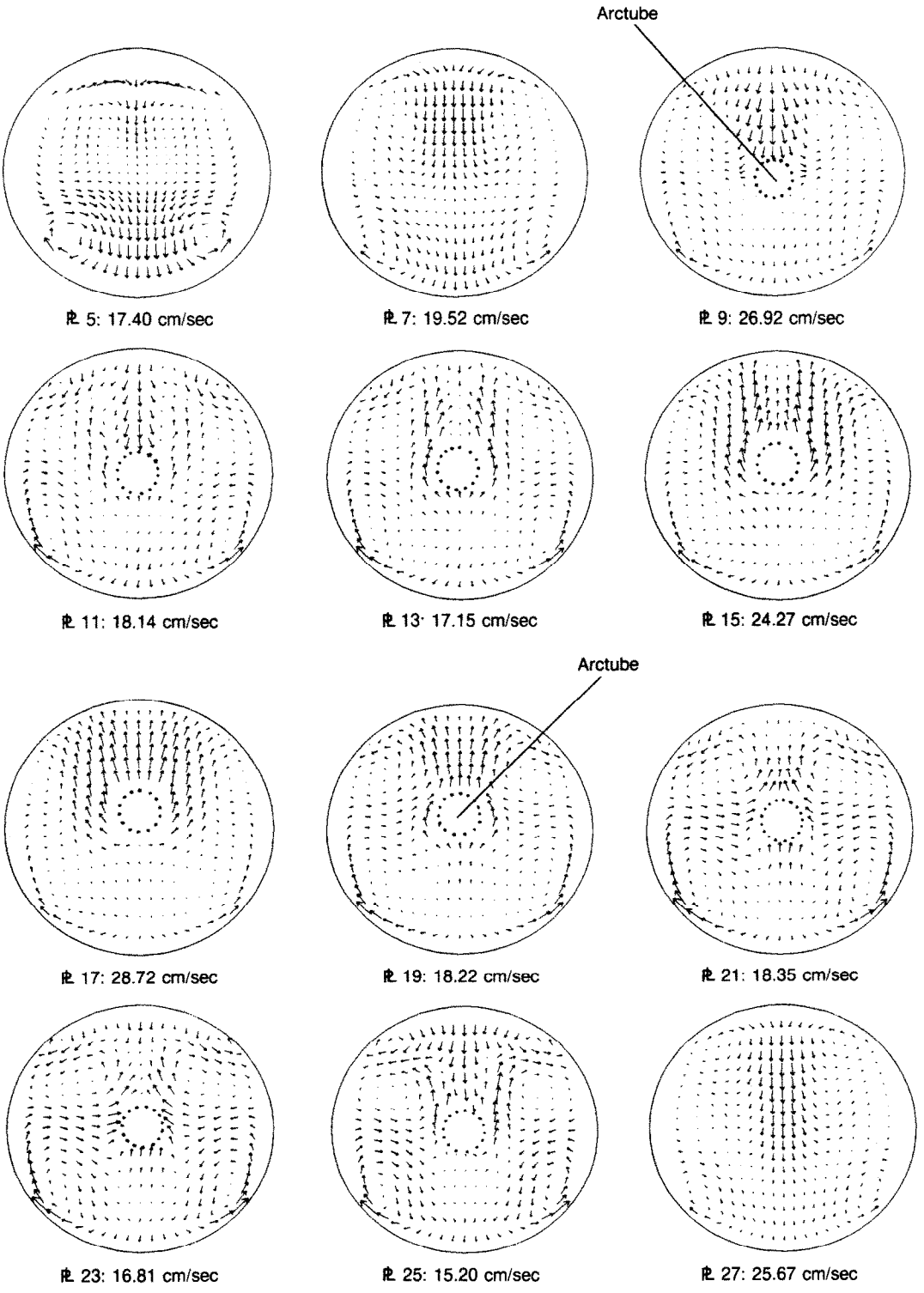

FIG. 10. Velocity vectors (and maximum vertical component values) on cross-view planes (from Plane No. 5 to 27) for operating pressure of 600 Torr.

the eddy structure developed in the side-view plane as already illustrated in Fig. 9. Due to the bending curvature of the arctube, the gap between the top walls of the arctube and jacket is minimum at the middle and increases toward the end regions. Consequently, the vertical temperature gradient is the highest in the middle region, and a thermal plume type of flow appears there. This structure dictates flow

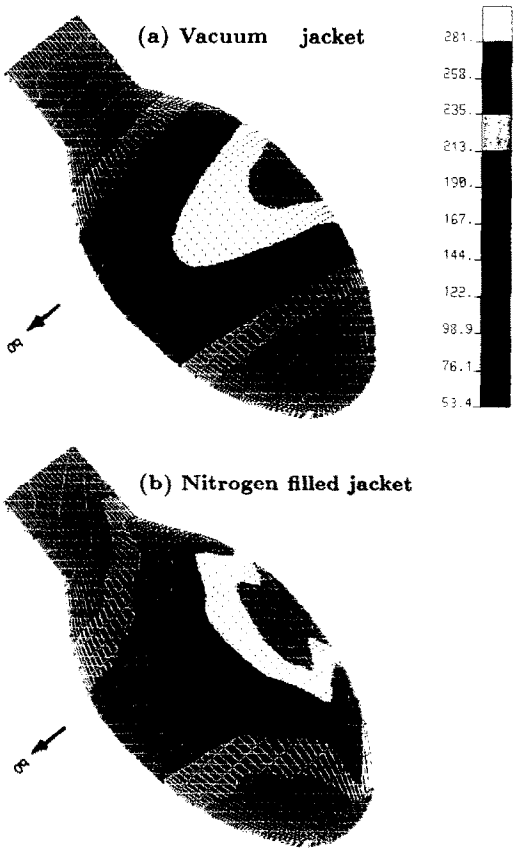

FIG. 11. Comparison of predicted outer wall temperature distributions between vacuum and nitrogen filled jackets.

development in other regions. In summary, the top wall temperature differences between the arctube and the jacket, combined with the variation of distance between them, are responsible for the overall convection structure depicted in Figs. 9 and 10. The other notable feature observable in Fig. 10 is that in all cross-view planes, two eddies appear in the two lower corner regions.

Finally, Fig. 11 shows a direct comparison of the overall outer wall temperature distributions between the vacuum and the nitrogen filled jackets based on the computations. With a vacuumed environment, as shown in Fig. 11(a), the wall temperature varies predominantly along the axial direction, as evidenced by the ring-like stripes of the isotherms. The exception is the top wall region above the middle of the arctube, where the arctube curvature creates a hot spot through radiation transfer. With a nitrogen filled jacket, as shown in Fig. 11(b), the wall temperature distribution is less regular. Since hot gas moves upward and cold gas moves downward, the bulk of the lower half jacket wall now appears cooler while the hot spot on the top wall becomes hotter. Compared to the case of the vacuum jacket, convection has produced a larger temperature variation along the circumferential direction and smaller temperature variation along the axial direction.

4. SUMMARY AND CONCLUSION

Both theoretical and experimental information has been presented regarding the heat transfer and fluid flow characteristics inside a discharge lamp. The following are the conclusions reached in the present study.

(1) Both convection and radiation contribute substantially to heat transfer between the arctube and the jacket. Their effects can be separated by studying evacuated and nitrogen filled jackets.

(2) The curvature of the arctube, originally designed to accommodate the thermal characteristics within the arctube, strongly affects both convection and radiation characteristics outside the arctube.

(3) A simple model comprising a radiating point source can be successfully utilized to represent the overall radiation heat transfer behavior between the arctube and the jacket. In the present configuration, experimental evidence suggests that the radiation flux inversely proportional to $r^{2.8}$ is a very good approximation for the present configuration.

(4) Convection within the jacket heats up the top wall while cooling down the bottom wall of the jacket. Increasing operating pressure distributes temperatures more uniformly inside the jacket as well as those on the jacket wall.

(5) The top wall temperature differences between the arctube and the jacket, combined with the variation of distance between them, are responsible for the observed overall convection structure.

The information presented here represents the first successful attempt at bringing together theoretical and experimental results to study the very complicated three-dimensional heat transfer and convection charcteristics within a modern discharge lamp. The theory/data validation provides confidence that the theoretical model employed here is correct. With improved knowledge of the physical processes involved in the lamp, design optimization can be performed for, e.g. different fill pressures and lamp sizes. Furthermore, different configurations can be designed according to changes of operating condition, such as in microgravity environments [10, 18], where the gravity induced convection heat transfer is unimportant relative to radiation effects.

Acknowledgments—We are grateful to acknowledge the contributions made by Mark Duffy, Jim Otlowski, Patrick Manney, and Rich Nagle for their efforts of making the special lamps and the wall temperature measurements. We would like to thank Jim Dakin for the discussion of the radiation model. Ongoing support and encouragement by Jack Strok are also much appreciated.

REFERENCES

1. W. Elenbass, *The High Pressure Mercury Vapor Discharge*. North-Holland, Amsterdam, The Netherlands (1951).

2. J. F. Waymouth, *Electric Discharge Lamps*. MIT Press, Cambridge, Massachusetts (1971).
3. C. Kenty, On convection currents in high pressure mercury arcs, *J. Appl. Phys.* **9,** 53–66 (1938).
4. R. J. Zollweg, Convection in vertical high-pressure mercury arcs, *J. Appl. Phys.* **49,** 1077–1091 (1978).
5. J. J. Lowke, Calculated properties of vertical arcs stabilized by natural convection, *J. Appl. Phys.* **50,** 147–157 (1979).
6. J. T. Dakin and W. Shyy, The prediction of convective and additive demixing in vertical metal halide discharge lamps, *J. Electrochem. Soc.* **136,** 1210–1215 (1989).
7. P. Y. Chang, W. Shyy and J. T. Dakin, A study of three-dimensional natural convection in high pressure mercury lamps—I. Parametric variations with horizontal mounting, *Int. J. Heat Mass Transfer* **33,** 483–493 (1990).
8. W. Shyy and P. Y. Chang, A study of three-dimensional natural convection in high pressure mercury lamps—II. Wall temperature profiles and inclination angles, *Int. J. Heat Mass Transfer* **33,** 495–506 (1990).
9. P. Y. Chang and W. Shyy, Adaptive grid computation of three-dimensional natural convection in horizontal high pressure mercury lamps, *Int. J. Numer. Meth. Fluids* **12,** 143–160 (1991).
10. W. Shyy and P. Y. Chang, Effects of convection and electric field on thermofluid transport in horizontal high pressure mercury arcs, *J. Appl. Phys.* **67,** 1712–1719 (1990).
11. W. Shyy, S. S. Tong and S. M. Correa, Numerical recirculating flow calculation using a body-fitted coordinate system, *Numer. Heat Transfer* **8,** 99–113 (1985).
12. M. E. Braaten and W. Shyy, A study of pressure correction methods with multigrid for viscous flow calculations in non-orthogonal curvilinear coordinates, *Numer. Heat Transfer* **11,** 417–442 (1987).
13. W. Shyy, S. M. Correa and M. E. Braaten, Computation of flow in a gas turbine combustor, *Combust. Sci. Technol.* **58,** 97–117 (1988).
14. J. R. Howell, Thermal radiation in participating media: the past, the present, and some possible futures, *J. Heat Transfer* **110,** 1220–1229 (1988).
15. C. Saltiel and M. H. N. Naraghi, Analysis of radiative heat transfer in participating media using arbitrary nodal distribution, *Numer. Heat Transfer* **17,** 227–243 (1990).
16. J. P. Holman, *Heat Transfer*, 5th Edn. McGraw-Hill, New York (1981).
17. Y. S. Touloukian, R. W. Powell, C. Y. Ho and P. G. Klemens, *Thermal Conductivity—Nonmetallic Solids*, Vol. 2 of *Thermophysical Properties of Matter*. Ifi/Plenum, New York (1970).
18. W. Shyy and P. Y. Chang, Transport process in horizontal discharge lamp under microgravity, *Int. Commun. Heat Mass Transfer* **16,** 713–722 (1989).

TRANSFERT THERMIQUE ET ECOULEMENT FLUIDE TRIDIMENSIONNELS DANS LES LAMPES A DECHARGE MODERNES

Résumé—Il est bien connu que les caractéristiques de convection et de transfert thermique peuvent affecter fortement la qualité de la lumière ainsi que la durée de vie d'une lampe à décharge. Néanmoins le niveau actuel de connaissance des mécanismes n'est pas suffisant pour guider les ingénieurs à cause des complexités physiques et géométriques. On a fait ici un effort expèrimental et théorique pour identifier les rôles des différents mécanismes de transfert de chaleur entre le tube d'arc et l'enveloppe d'une lampe à décharge moderne. En résolvant les équations tridimensionnelles de Navier–Stokes et en simplifiant la modélisation du rayonnement en coordonnées curvilignes, on obtient un bon accord entre les mesures et les prédictions en ce qui concerne les profils de température de paroi. On a trouvé que les modes convectifs et radiatifs sont importants dans le transfert global de chaleur. Le modèle théorique montre en détail les relations entre les gradients de température et les variations géométriques autour du tube d'arc et leur impact sur la structure du champ de convection.

DREIDIMENSIONALE VORGÄNGE VON WÄRMEÜBERGANG UND STRÖMUNG IN EINER MODERNEN ENTLADUNGSLAMPE

Zusammenfassung—Es ist hinreichend bekannt, daß Wärmeübergang und Konvektion die Qualität des Lichtes ebenso beeinflussen wie die Lebensdauer einer Entladungslampe. Der heutige Wissensstand über diese Vorgänge ist aufgrund der physikalischen und geometrischen Komplexität noch nicht dazu geeignet, Auslegungsregeln anzugeben. In der vorliegenden Arbeit werden sowohl experimentelle als auch theoretische Anstrengungen unternommen, die Einflüsse der verschiedenen Wärmeübertragungsmechanismen in einer modernen Entladungslampe anzugeben. Durch Lösen der dreidimensionalen Navier–Stokes-Gleichungen und durch Verwendung eines vereinfachten Strahlungsmodells mit gekrümmten Koordinaten wird eine gute Übereinstimmung zwischen gemessenen und berechneten Wandtemperaturverteilungen erzielt. Sowohl Konvektion als auch Strahlung spielen beim Gesamtwärmeübergang eine wichtige Rolle. Das Zusammenwirken zwischen Temperaturgradienten und geometrischer Anordnung der Umgebung des Lichtbogens sowie ihr Einfluß auf die Struktur des Strömungsfeldes in der Entladungslampe werden von dem theoretischen Modell ebenfalls detailliert beschrieben.

ТРЕХМЕРНЫЙ ТЕПЛОПЕРЕНОС И ТЕЧЕНИЕ ГАЗА В СОВРЕМЕННОЙ ГАЗОРАЗРЯДНОЙ ЛАМПЕ

Аннотация—Как известно, характеристики теплопереноса и конвекции могут оказывать существенное влияние на яркость свечения, а также на предполагаемый срок службы газоразрядной лампы. Однако современный уровень понимания этих процессов не является достаточным для инженерной разработки в силу имеющихся физических и геометрических сложностей. В настоящем исследовании сделаны попытки экспериментального и теоретического определения роли различных механизмов теплопереноса между разрядной трубкой и кожухом газоразрядной лампы. При решении в криволинейных координатах трехмерных уравнений Навье–Стокса с использованием упрощенной модели излучения получено хорошее согласие между экспериментальными и теоретическими результатами для температурных профилей стенки. Найдено, что как конвекция, так и излучение являются важными факторами суммарного теплопереноса. При помощи теоретической модели выявлена взаимосвязь между температурными градиентами и изменениями геометрических параметров системы.